Siloxane-based metal–organic frameworks with remarkable catalytic activity in mild environmental photodegradation of azo dyes

Carmen Racles*, Mirela-Fernanda Zaltariov*, Mihail Iacob, Mihaela Silion, Mihaela Avadanei, Alexandra Bargan

"Petru Poni" Institute of Macromolecular Chemistry, Aleea Gr. Ghica Voda 41A, 700487 Iasi, Romania

A B S T R A C T

Three new metal–organic frameworks (MOFs) were obtained from a siloxane dicarboxylic acid (CX), 4,4′-bipyridyne (BPy) or 1,2-bis(4-pyridyl)ethylene (EBPy) and copper or cobalt acetates. The compounds were characterized by IR spectroscopy, powder X-ray diffraction, energy-dispersive X-ray fluorescence (XRF), thermogravimetric analysis (TGA), dynamic water vapor sorption (DVS), electron microscopy (TEM, SEM), UV–vis diffuse reflectance and fluorescence measurements. These hydrophobic MOFs acted as efficient catalysts in two processes occurring in aqueous media. The best result in alkaline decomposition of hydrogen peroxide was 90% conversion after 30 min. The catalytic activity in photodecomposition of Congo Red (CR) was followed in mild environmental conditions, i.e. under natural sunlight, without additional oxidation agents or pH adjustments. Unprecedented catalytic activity was found, especially for the Co complex with CX and EBPy, with discoloration efficiency of ca. 82% after 80 min of exposure to sunlight. The obtained results, in terms of rate constants and efficiency are comparable with those reported for other catalytic systems in photoreactors or in the presence of H_2O_2. The best catalyst was also tested in a Fenton-like process and it was found that the addition of H_2O_2 doubles the rate constant and increases the efficiency to 97%. On the other hand, the remaining waters after CR photodecomposition were analyzed by mass spectrometry (ESI–MS) and it was concluded that "cleaner" water is obtained when the MOFs are used without addition of H_2O_2.

1. Introduction

Metal–organic frameworks MOFs (coordination networks or coordination polymers), "the fastest growing class of materials today" [1] consist of metallic nodes linked by polytopic bridging linkers, being in fact hybrid inorganic–organic materials [2–5]. The constant interest in such structures derives from their outstanding potential in gas or solvents sorption [6–17], separation of gases [13,18], sensors [19–21] and catalysis [22–25]. They may also exhibit magnetic properties [26,27] or second order nonlinear optical (NLO) properties [28].

The remarkable properties of MOFs, their rational design according to particular requirements, their distinct architectures, their high specific area and porosity, which allow fast mass transport and/or interactions with substrates, make them

ideal materials used in catalysis [29]. A wide diversity of MOFs have been designed with various homo- and heterometallic ions or clusters and different ligands (carboxylic and N-donor ones), and screened in heterogeneous catalysis [30–33] as eco-friendly alternatives in a variety of organic transformations: oxidation of alcohols, hydrocarbons, sulfides, thioethers or olefins, Friedel-Crafts alkylation, hydrogenation of olefins, Suzuki-Miyaura coupling, cyanosilylation, acetalization and hydroformylation or ring-opening polymerization [34,35]. Of particular importance for environmental remediation is the removal of various contaminants, such as antibiotics or dyes, from wastewaters, where hybrid materials containing MOFs are promising materials, acting as adsorbents and photocatalysts [36,37].

The photodegradation of azo dyes from wastewaters is a very actual environmental topic, since these dyes are toxic and even carcinogenic. Congo Red (CR), extensively used in textile industry due to its affinity for cellulose, is an anionic azo dye with an aromatic structure, containing two azo groups and it is considered a very stable molecule [38]. Besides physical methods, chemical processes

* Corresponding authors.
E-mail addresses: raclesc@icmpp.ro (C. Racles), zaltariov.mirela@icmpp.ro (M.-F. Zaltariov).

such as ozonation and chlorination are frequently used for removal of textile dyes [39]. A range of materials have been tested as heterogeneous photocatalysts for azo dyes degradation, the most used being TiO_2 in different forms and combinations [40], to enhance its effect or to ease its removal [39,41,42]. Other materials have also been proposed for azo dyes degradation, in particular for Congo Red, as for example chitosan-CdS nanocomposites [43], Zn oxide [44–46], CuInSe2–ZnO nanocomposites [38], Zn sulfide [47], rare-earth doped nickel ferrites [48]. Generally, the photodegradation of azo dyes is conducted in photoreactors, under artificial UV irradiation, but the effect of sunlight have also been tested [49,50], as well as other energy sources, such as ultrasounds [42] and gamma irradiation [51], or biochemicals, such as enzymes [52].

In particular, the utility of MOFs as heterogeneous catalysts in photodegradation reactions proved to be very advantageous especially due to their high efficiency, ambient operating temperature, good reproductibility and catalyst reusability, easy handling and simplicity in degradation of persistent, nonbiodegradable and toxic organic dyes, without leaving secondary pollution products [53,54]. Efficient MOF photocatalysts for degradation of organic pollutants have been reported since 2006 [55]. More recently, numerous Ag, Zn, Cd, Fe, Ni, Cu, Mn and Co-based MOFs catalysts active in the decomposition of dyes have been reported, some of them having good photocatalytic performance for the degradation of: methylene blue, methyl orange, rhodamine B, reactive red, methyl red or methyl violet [53].

Relatively few reports have been published on catalytic efficiency of MOFs in the decomposition of Congo Red. Co, Zn or Cu-based MOFs built on mixed ligands (aromatic polycarboxylic acids and flexible N-donor ligands: pyrazole, imidazole, bezimidazole or pyridyl derivatives) were found as active heterogeneous catalysts for photodecomposition of Congo Red with a degradation efficiency of 55–99% depending on the reaction conditions (temperature, pH, irradiation light source, etc) [56–61]. Most of these reports describe heterogeneous Fenton-like process which uses H_2O_2 and UV lamp and/or high-pressure mercury-vapor lamp to generate hydroxyl radicals that are very effective in degrading such contaminants. The photocatalytic degradation of Congo Red under visible light, with MOFs without oxidation agents like H_2O_2 was rarely studied [59].

One of the most reliable methods for the synthesis of coordination polymers is the mixed-ligand synthetic strategy [62]. In this approach, typical building blocks are bipyridine and polycarboxyl compounds, often as acid-base mixed-ligands. Numerous coordination polymers of different transition metals on the base of ligands containing both COOH and pyridyl groups have been reported [3,4]. In our group, a special attention has been given to the use of siloxane-based ligands, as flexible and hydrophobic bridging elements for a wide range of MOFs [63–66]. The hydrophobicity of these MOFs due to the presence of the tetramethyldisiloxane moieties in their structures (which can protect MOFs from degradation upon contact with water) is a big advantage for their stability and use as heterogeneous catalysts in aqueous medium, because it is well known that the majority of MOFs are usually not stable in water [67,68]. Also, such MOFs can be regarded as amphiphilic compounds, which could support molecular interactions favorable to the catalytic reactions [69]. Some of the siloxane-containing metal complexes have been tested in catalysis applications, for aerobic oxidation of benzyl alcohol to benzaldehyde [70], hydrocarboxylation of linear and cyclic alkanes, oxidation of cyclohexane, and of 1-phenylethanol [71,72].

In a previous paper [73] we reported on Zn coordination polymers (2D MOF structures) obtained by mixed-ligand method, starting from 1,3-bis(3-carboxypropyl)-tetramethyldisiloxane (CX) and 4,4′-bipyridyl or 1,2-bis(4-pyridyl)ethylene as the base component. The Zn MOFs have been tested as catalysts in hydrogen peroxide

decomposition. This is another interesting application, since H_2O_2 is an environmentally friendly oxidation agent, which provides a clean and safe reaction path, being used in the oxidation of alcohols and biopolymers, including cellulose bleaching [74].

Here we report on similar compounds obtained with Co and Cu, their catalytic activity in hydrogen peroxide decomposition and in photodegradation of Congo Red under ambient conditions. The efficiency of Co and Cu catalysts in H_2O_2 decomposition clearly surpassed the Zn homologues reported previously. The decomposition of CR in the absence of additional oxidation agents occurred with similar rate as with core-shell $ZnO@\gamma - Fe_2O_3$ nanocomposites [49], with a remarkable color removal efficiency of 81% after 80 min. A Fenton-like catalytic system was also tested, which showed higher reaction rate and 97% efficiency. The ESI–MS analysis suggested a higher level of the dye decomposition process in reactions catalyzed by MOFs without H_2O_2. Compared to other reports, in this case the proposed decontamination method is overall less energy-consuming. First of all, the synthesis of the metal complexes is facile, occurring at ambient temperature. The dye decomposition (decontamination of wastewaters) involves easily removable solid catalysts, without additional corrosive agents or neutralization steps and it occurs under natural light and ambient temperature, followed by simple filtration for the recovery of the catalyst. Due to the high stability of the MOFs, no trace of metal was detected in purified water. In addition, UV light might negatively affect the living organisms, thus the use of natural light in decontamination processes is of outmost importance. To our knowledge, this is the first report on hydrophobic MOFs acting as efficient catalysts in water decontamination.

2. Experimental

2.1. Materials

1,3-bis(3-carboxypropyl)tetramethyldisiloxane, [HOOC$(CH_2)_3(CH_3)_2$Si]$_2$O (CX) was synthesized using a reported method [75]. 4,4′-bipyridine (BPy), 1,2-bis(4-pyridyl)ethylene (EBPy), DMF and THF (from Fluka), cobalt(II) acetate, Co(OCOCH$_3$)$_2$·4H$_2$O and copper(II) acetate Cu(OCOCH$_3$)$_2$·H$_2$O (from Chimopar S.A) were high purity compounds and were used as received.

2.2. Methods

The infrared (IR) spectra were registered on a Bruker Vertex 70 FT-IR instrument, in transmission mode, in the 400–4000 cm^{-1} range (resolution 2 cm^{-1}, 32 scans), at ambient temperature. Far IR spectra were recorded using the same spectrometer equipped with a FIR source, CsI beamsplitter and standard DLaTGS detector. Spectra were obtained in the transmission mode in the range 180–700 cm^{-1} at room temperature with a resolution of 2 cm^{-1} and accumulation of 64 scans.

Thermogravimetric analyses (TG-DTG-DTA) were performed on an STA 449F1 Jupiter NETZSCH (Germany) equipment. The measurements were made in the temperature range 20–700 °C under a nitrogen flow (50 mL/min) using a heating rate of 10 °C/min. Alumina crucibles were used as sample holders. Qualitative optical observations were done with an Olympus polarized light optical microscope.

The energy-dispersive X-ray fluorescence (XRF) system (EX-2600 X-Calibur SDD) was used to determine the presence and ratio of metal (Co or Cu) and Si in the structure of the coordination polymers. TEM investigations were made with Hitachi High-Tech HT7700 Transmission Electron Microscope, operated in high contrast mode at 100 kV accelerating voltage. Samples were

cast from diluted and sonicated aqueous dispersion on 300 mesh carbon coated copper grids and vacuum dried. For overall assessment of the samples aspect, the finely grounded powders were analyzed with an Environmental Scanning Electron Microscope (ESEM) type Quanta 200, operating at 30 kV with secondary electrons. The Energy Dispersive X-Ray system (EDX) of the SEM was used for qualitative and semi-quantitative analysis, the materials being pressed into pellets and glued on carbon tape for this analysis.

Powder X-rays Diffraction (PXRD) analysis was performed on a Bruker-AXS D8 ADVANCE diffractometer, with Bragg Brentano parafocusing goniometer, working at 40 kV and 30 mA tube power. Scans were recorded in step mode using Ni-filtered Cu Ka radiation ($\lambda = 0.1541$ nm).

The sorption capacity of water vapors (DVS) was measured in dynamic regime at 25 °C (298 K) in the relative humidity range RH 0–90% by using an IGAsorp equipment (Hiden Analytical, Warrington UK). The vapor pressure was increased and decreased in 10% humidity steps between 0 and 90% RH for sorption and reverse for desorption, each having a pre-established equilibrium time between 10 and 20 min.

Mass spectrometry data were obtained using an Agilent 6520 Series Accurate-Mass Quadrupole Time-of-Flight (Q-TOF) LC/MS. The solutions were introduced into the electrospray ion source (ESI) via a syringe pump at a flow-rate of 0.01 mL/min. After optimization of the Q/TOF MS parameters, they were set as follows: electrospray ionization (positive ion mode), drying gas (N_2) flow rate 7 L/min; drying gas temperature 325 °C; nebulizer pressure 15 psig, capillary voltage 4500 V; fragmentation voltage 200 V; the full-scan mass spectra of the investigated compounds were acquired in the m/z range of 100–1500. The mass scale was calibrated using the standard calibration procedure and compounds provided by the manufacturer. Data were collected and processed using MassHunter Workstation Software Data Acquisition for 6200/6500 Series, version B.01.03.

Electronic absorption spectra of CR solutions were measured by using a Jenway 6505 **S**pectrophotometer (Watford, UK) in 10 mm optical path polystyrene cells. UV–vis absorption spectra measurements of the catalysts in solid state were carried out using the diffuse reflectance accessory on a Specord 200 spectrophotometer. Spectralon® was used as reference. The optical band gaps of the free ligands and MOFs were determined from the diffuse reflectance spectra. In order to determine the optical band gap, the diffuse reflectance spectra (DR) were converted in absorbance by using Kubelka – Munk function $F(R_\infty) = \left[(1 - R_\infty)^2\right] / [2 R_\infty]$, where R_∞ is reflectance of the sample with infinite thickness. Replacing the absorption coefficient in the Tauc's power-law relationship with $F(R_\infty)$, the following expresion is used for determining the optical band gap $F(R_\infty) \times h\nu = A \left(h\nu - E_g\right)^m$, where m is 1/2 or 2 for materials with direct or indirect band gap, respectively, and A is a material constant [76]. For the materials with a direct band gap, extrapolating the linear part of the plot $[F(R_\infty) \times h\nu]^2$ vs. photon energy $h\nu$ to the energy axis allows determining the value of E_g.

Fluorescence spectra were obtained by using a Perkin Elmer LS55 luminescence spectrometer in solid state.

2.3. Synthesis of the complexes

Stoichiometric amounts of CX and bipyridine compounds were first mixed in THF to afford the corresponding H-bond supramolecular polymer ligands (A and B) [73]. After solvent removal, the resulted polymer was dissolved in DMF and mixed in stoichiometric amounts with the metal acetates as DMF solution at room temperature. Bulky precipitates formed instantly, which were filtered and washed with DMF, then dried. The metal complexes resulted from the reaction with 4,4′-bipyridine were coded Co-A and Cu-A, while

the compound obtained with 1,2-bis(4-pyridyl)ethylene was coded Co-B. Repeated attempts to obtain single crystals by solvothermal method, in DMF/water or ethanol/water systems were unsuccessful.

Cu-A (turquoise powder): IRν_{max} (KBr), cm^{-1}: 3438w, 3071vw, 2955m, 2928w, 2899w, 2878w, 1619vs, 1539w, 1489w, 1419s, 1318m, 1253s, 1220m, 1170w, 1128w, 1070s, 971vw, 889w, 839s, 795s, 734w, 682w, 630w, 618w, 572vw, 509vw.

Far IR ν_{max} (KBr), cm^{-1}: 629vw, 575vw, 557, 523vw, 262vs, 231m, 208s.

XRF: Cu:Si atomic ratio 0.56:1.

Co-A (pink powder): IRν_{max} (KBr), cm^{-1}: 3416s, 3074vw, 3046vw, 2957m, 2926m, 2899w, 1605vs, 1558vs, 1489m, 1437s, 1414vs, 1339w, 1317w, 1256s, 1219w, 1171w, 1067s, 1047s, 935vw, 910vw, 883w, 839s, 816s, 797s, 733w, 671m, 629m, 511w, 476w, 399w.

Far IR ν_{max} (KBr), cm^{-1}: 673w, 627m, 573vw, 480vw, 338vw, 253s, 230vs.

XRF: Co:Si atomic ratio 1.1:1.

Co-B (pink powder): IRν_{max} (KBr), cm^{-1}: 3416w, 3063vw, 3011 v, 2953m, 2924w, 2872w, 1607vs, 1568s, 1501w, 1435s, 1317w, 1252m, 1219w, 1178, 1124w, 1053s, 1016m, 986m, 889w, 835s, 793m, 669w, 619w, 554m.

Far IR ν_{max} (KBr), cm^{-1}: 671m, 646w, 617m, 584vw, 554vs, 505vw, 471vw, 316w, 260s, 231m, 212w, 191vw.

XRF: Co:Si atomic ratio 1:1.

2.4. Hydrogen peroxide decomposition

Catalytic tests for hydrogen peroxide decomposition, in alkaline medium were done using the gasometric technique [77]. In principle, the O_2 formed according to Eq. (1) displaces water from a Bunte gas burette. The experiments were done at atmospheric pressure and 300 K. The catalyst (around 2.5 mg) and a 4N NaOH solution were mixed together for 15 min, then 15% H_2O_2 was added (10/1 vol. ratio) and the oxygen evolution was monitored till no modification was noticed. A blank experiment was done in the same conditions.

$$2HO_2^- = O_2 + 2OH^- \tag{1}$$

2.5. Photodegradation of Congo red

Congo Red aqueous solution (3 mL, 50 mg L^{-1}) was placed in disposable UV cells, which were capped and stored in the dark. In each cell around 3 mg of catalyst was added, except one which was the reference (blank sample). The cells were manually shacked, then they were exposed to direct sunlight for certain time intervals. The UV–vis spectra were measured after each exposure, and the samples were stored in the dark during manipulation. For Fenton-like experiments, 25 μL of H_2O_2 were added to the CR solution containing the catalyst Co-B or to the reference and the same procedure was applied.

3. Results and discussion

3.1. Synthesis and characterization of the MOFs

By reacting CX, BPy or EBPy, and metal acetates (Cu, Co), the compounds Co-A, Cu-A and Co-B were obtained as polycrystalline powders (Scheme 1). Unfortunately, these were not soluble to allow subsequent recrystallization as single crystals, as in the case of our previously reported Zn complexes [73].
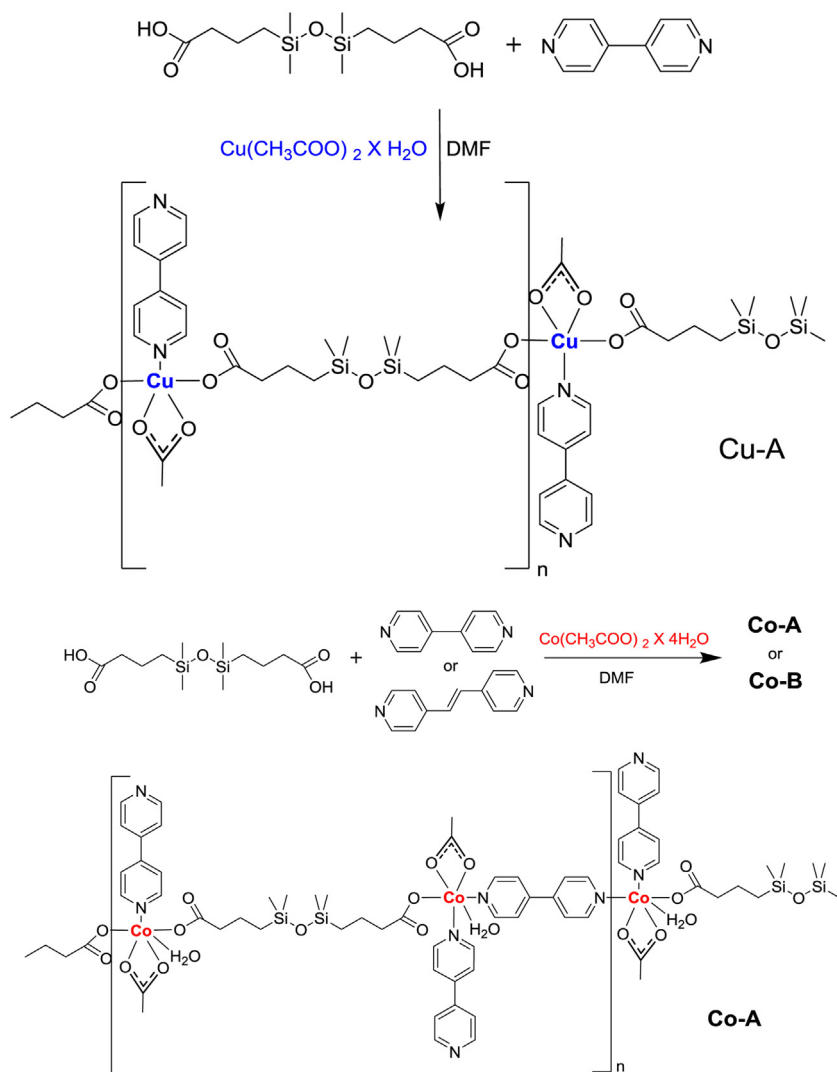
Scheme 1. Synthesis and possible structure of the metal complexes.

3.1.1. FT-IR spectroscopy

The formation of the complexes was confirmed by FT-IR, which allowed the assignment of the most important features in their structure based on literature data and our previous results. The mode of the carboxylate binding was assigned by the level of the separation between the asymmetric and symmetric stretches ($\Delta = \nu_{as}(COO^-) - \nu_s(COO^-)$, where $\Delta_{chelating} < \Delta_{bridging} < \Delta_{ionic} < \Delta_{monodentate}$, the value of Δ_{ionic} being approximately $164\,cm^{-1}$ for acetates [78].

The overlapped and hidden peak positions of the caboxylate and acetate $\nu_{as}(COO^-)$ and $\nu_s(COO^-)$ stretches for the compounds Cu-A, Co-A and Co-B were determined with the second derivative of the spectra. The COO— stretching vibration regions $1700–1500\,cm^{-1}$ and $1480–1360\,cm^{-1}$ were deconvoluted by a curve-fitting method and the areas were calculated with a 50% Lorentzian and 50% Gaussian function. The curve-fitting analysis was performed with OPUS 6.5 software. The procedure led to a best fit of the original curve with an error of less than 0.001 (Fig. 1).

The FT-IR spectrum of Co-A showed the specific bands for the starting siloxane compound: $1255\,cm^{-1}$ (δ sym Si-CH$_3$), $1067\,cm^{-1}$ (Si-O-Si asymmetric stretch), $839\,cm^{-1}$ (γ Si-(CH$_3$)$_2$), the hetero-aromatic band at $1606\,cm^{-1}$, as well as the newly formed carboxylate bands: asymmetric at $1580\,cm^{-1}$ and symmetric at $1414\,cm^{-1}$. Based on these bands ($\Delta(\nu_{as} - \nu_s) = 166\,cm^{-1}$)

and on those observed in the sodium salt of CX, taken as the reference ionic combination ($\Delta(\nu_{as} - \nu_s) = 139\,cm^{-1}$), the carboxylic acid groups act as monodentate ligand in this metal complex [78]. In addition, absorption bands at 1548 and $1437\,cm^{-1}$ could be assigned to acetate ν_{as} and ν_s, respectively. In this case, the difference in wavenumber is less than in the corresponding ionic combination which confirms the presence of the acetate group as bidentate chelating ligand. Based on these data, it is reasonable to assume that Co-A compound contains both acid ligands. Similar infrared spectra were recorded for the other two complexes (Fig. 1), with carboxylate bands for Cu-A at: 1566, $1418\,cm^{-1}$ (CX monodentate) and 1539, $1445\,cm^{-1}$ (acetate bidentate) and for Co-B, respectively at: 1568, $1411\,cm^{-1}$ (CX monodentate), 1548, $1440\,cm^{-1}$ (acetate bidentate). Other characteristic bands in these spectral regions are assigned to the stretching vibrations, in-plane or out-of –plane deformations of the aliphatic and aromatic C—H, C=C, CH=N, C—N groups: $\delta(CH_3) + \delta(CH_2)$ at $1454\,cm^{-1}$ (Cu-A and Co-A), C=C stretching at $1620\,cm^{-1}$ (Cu-A), 1668 and $1628\,cm^{-1}$ (Co-A), aromatic C=N at $1603\,cm^{-1}$ (Cu-A), $1606\,cm^{-1}$ (Co-A and Co-B), =C—H in-plane bending at 1430 and $1400\,cm^{-1}$ (Cu-A) and $1404\,cm^{-1}$ (Co-A) [79].

In the far infrared region of the synthesized compounds the characteristic vibrations for Cu—N and Co—N coordination bonds at 262 and $231\,cm^{-1}$ (Cu-A), 253 and $230\,cm^{-1}$ (Co-A) and 316,
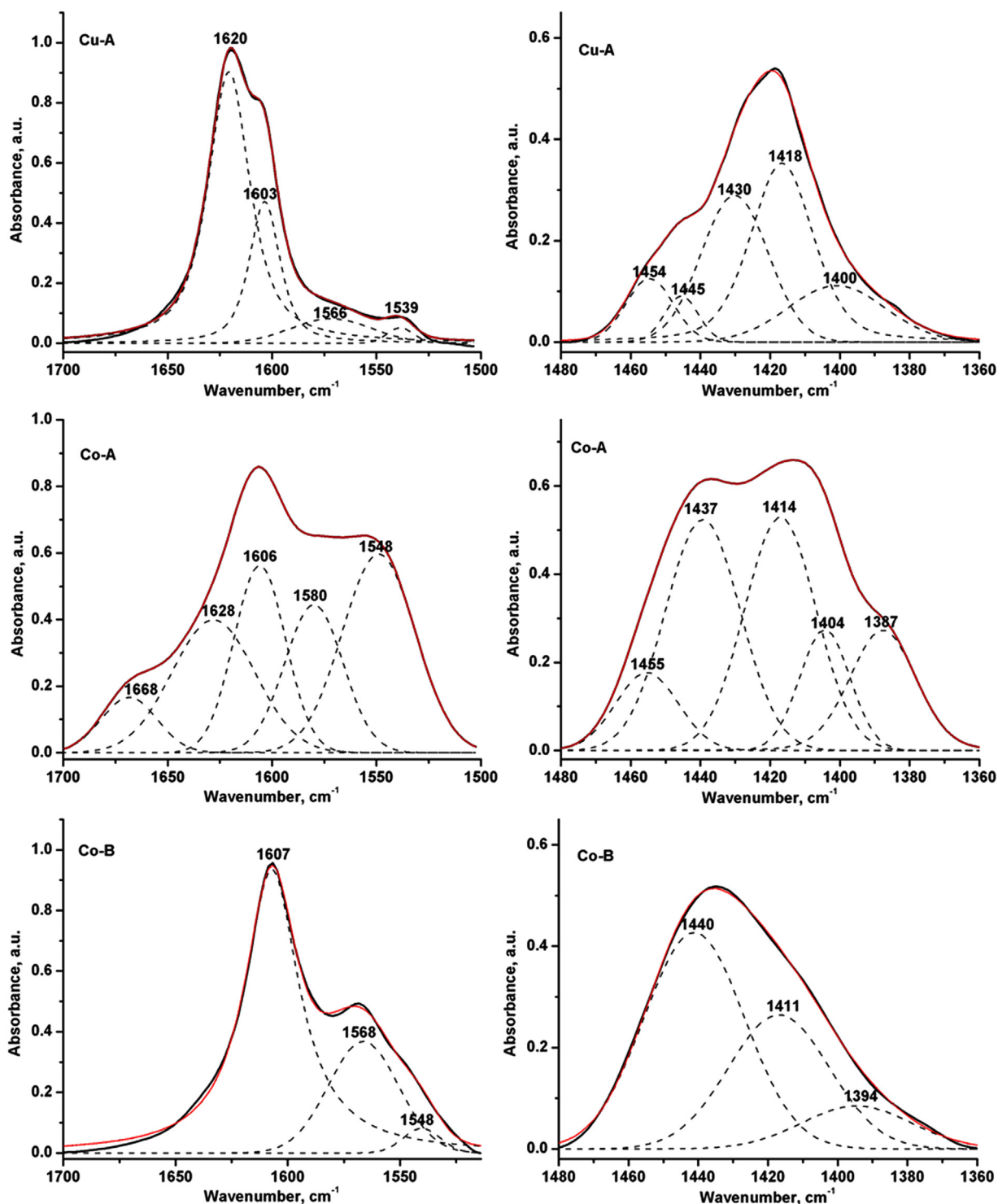
Fig. 1. Deconvoluted FTIR spectra in the range 1700–1500 cm^{-1} and 1480–1360 cm^{-1} for Cu-A, Co-A and Co-B.

260 and 231 cm^{-1} (Co-B) and those assigned to Cu-O and Co-O (carboxylate and acetate) at 557 and 575 cm^{-1} (Cu-A), 480 and 573 cm^{-1} (Co-A), 554 and 584 cm^{-1} (Co-B) can be seen, which confirms that the coordination of the metal ions occurs by both, oxygen and nitrogen atoms (Fig. 1S) [78].

3.1.2. Energy dispersive X-ray analysis

Silicon and metal (Co or Cu) were detected by XRF spectroscopy (Fig. 2) and SEM/EDX (Fig. 2S). For the Co MOFs, the detected Co:Si atomic ratio was ~1:1, which indicates a 2/1 molar ratio between the metal and the disiloxane ligand. SEM/EDX confirmed this ratio and showed a N:Co atomic ratio of ~1.5:1. Thus, taking into account FT-IR and EDX data, and assuming the (typical) coordination number 6 for Co ions, the composition of the Co complexes could be depicted as $[Co_2(CX)(BPy)_{1.5}(Ac)_2]\cdot 2H_2O$ and $[Co_2(CX)(EBPy)_{1.5}(Ac)_2]\cdot 2H_2O$ respectively (Scheme 1). For Cu-A, the Cu/Si atomic ratio (from XRF and EDX) was 0.56, indicating the presence of one disiloxane ligand for each metal center. The N:Cu atomic ratio is 1:1, thus we proposed a structural unit with the formula: $[CuCX(BPy)_{0.5}(Ac)]$ (Scheme 1, Fig. 3S).
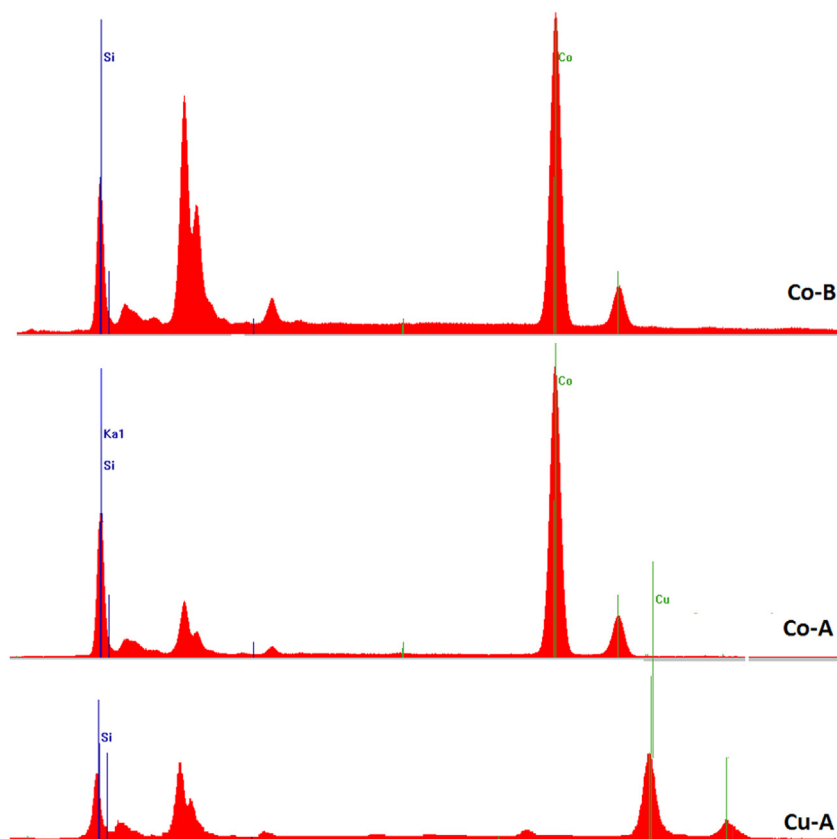
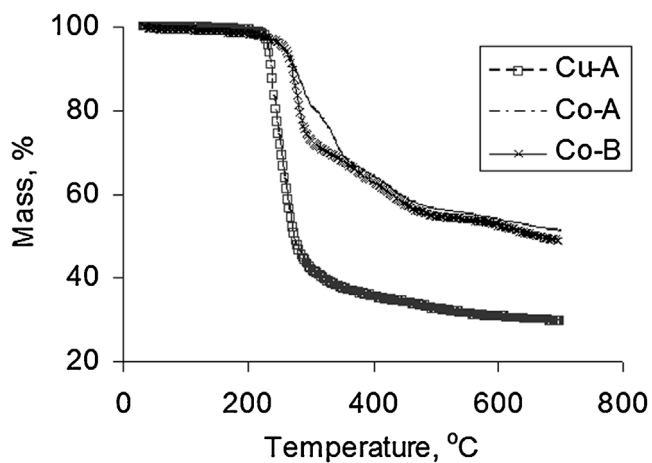**Fig. 2.** XRF spectra of the metal complexes.

Fig. 3. TGA curves of the metal complexes.

3.1.3. Thermal stability

DSC/DTA analysis was used to verify the purity of the obtained materials. Un-reacted ligands were not observed by optical microscopy or by DSC (knowing that CX melts at 50 °C, BPy at 114 °C, and EBPy at 148–150 °C).

TGA in nitrogen was used to assess the thermal stability of all the coordination compounds. Better thermal stability was observed for Co complexes, with temperature corresponding to 10% weight loss (T_{10}) of around 280 °C, compared to Cu-A with T_{10} of around 240 °C. The residual mass was around 50% for the Co complexes and 30% for the Cu complex (Fig. 3).

3.1.4. Morphology and powder XRD analysis

Scanning electron microscopy (Fig. 4a–c) showed microcrystalline powders with unitary aspect, uniform granulation and different morphology: spherulites (grains) in Cu-A, 3D porous structure in Co-A and needle crystals in Co-B. Morphology details were revealed by TEM from diluted and sonicated dispersions (Fig. 4d–f), showing different shape of the constitutive grains: quasi-spherical particles (spherulites) in Cu-A, cubic crystallites in Co-A, and rod-like in Co-B.

The powder XRD spectra (Fig. 5) indicate crystalline materials. The main diffraction peaks and the corresponding d Bragg distances are collected in Table 1S. The crystallite size was calculated with Scherrer's equation for the two samples with quasi-spherical (Cu-A) or cubic (Co-A) shape of the structural elements, as observed in TEM. The found values were 22.4 nm and 24.2 nm, respectively, which represent the mean size of the ordered domains and are in agreement with the smallest size of the grains observed in TEM.

Analyzing the ratio of the peak positions in the low-medium angle region which reflects the supramolecular organization, a periodicity of 1:2:3:4 was found for Cu-A and Co-B indicating layered supramolecular structures. For Co-A, a periodicity of $1:\sqrt{2}: \sqrt{3}: 2:\sqrt{5}...$ was identified, characteristic for a cubic lattice [80].

3.1.5. Water vapors sorption

DVS was used to evaluate the hydrophilic behavior, in isothermal measurements of water vapor sorption capacity. The results indicate low sorption capacity, with maximum weight gained of 1.6–2.9% (Table 1) and a type V adsorption isotherm, (according to the IUPAC classification) corresponding to hydrophobic or low hydrophilic materials with low sorption at low *RH*, moderate sorption at the middle *RH* and high water sorption at *RH* in close proximity to 100 (Fig. 4S). This type of isotherm is associated with
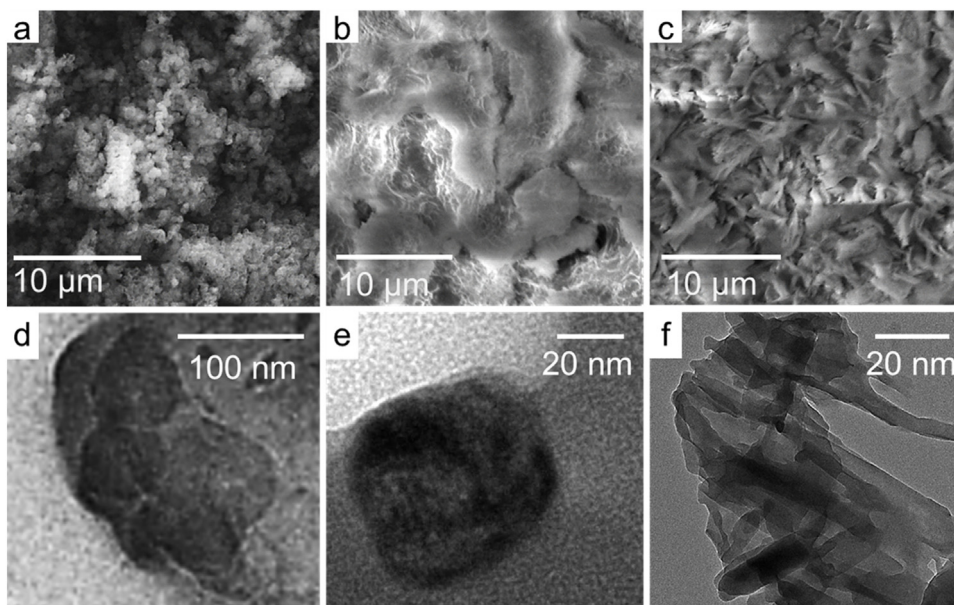
Fig. 4. Electron microscopy images of the MOFs: SEM of Cu-A (a), Co-A (b) and Co-B (c); TEM of Cu-A (d), Co-A (e) and Co-B (f).

Table 1
DVS data and estimated values of parameters of the GAB and BET models.

Sample	W (%)[a]	The average pore size r_{pm} (nm)	BET analysis		GAB analysis	
			A_{BET} (m²/g)	Monolayer, W_m (g/g)	A_{GAB} (m²/g)	Monolayer, W_m (g/g)
Cu-A	2.8788	2.81	20.459	0.005827	22.419	0.006385
Co-A	2.0172	1.40	28.874	0.008224	–	–
Co-B	1.5703	2.23	14.073	0.004008	13.531	0.003854

[a] Weight of water adsorbed, reported to dry basis.
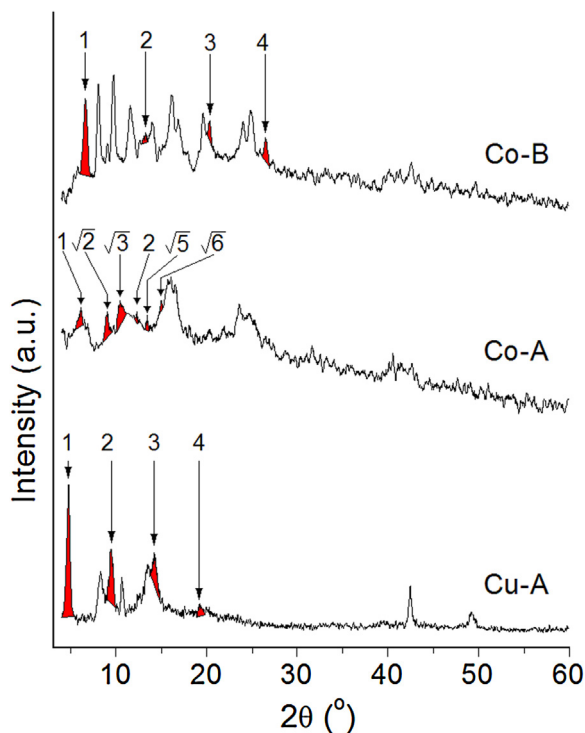

Fig. 5. Powder XRD spectra of the metal complexes.

weak fluid-solid interactions and represents adsorption isotherm with hysteresis, characteristic for porous solids. Very important features of the metal-organic frameworks are their pore size and surface area. Although these parameters are usually obtained in nitrogen sorption experiments, we used DVS to have an estimate and comparison between samples. This method has been used in other cases for estimating the surface areas and the average pore size of materials [66,81,82]. On the other hand, as our intention was to use these compounds as catalysts in aqueous medium reactions (H_2O_2 decomposition, dyes photodegradation), their behavior in contact with water vapors would be of primary importance, as well as the parameters derived from water sorption.

Both Brunauer-Emmett-Teller (BET) and Guggenheim-Anderson-de Boer (GAB) methods were used for evaluating the surface area based on water vapor sorption data. These models are very often used for modeling of the sorption isotherms and are based on Eq. (2) for BET and (3) for GAB analysis.

$$W = \frac{W_m \cdot C \cdot RH}{(1 - RH) \cdot (1 - RH + C \cdot RH)} \quad (2)$$

$$W = \frac{W_m \cdot C \cdot K \cdot RH}{(1 - K \cdot RH) \cdot (1 - K \cdot RH + C \cdot K \cdot RH)} \quad (3)$$

Where: W – weight of sorbed water,
W_m – weight of water forming a monolayer,
C – sorption constant,
RH – relative humidity
K – additional constant for the GAB equation.

BET Eq. (2) is considered as a special case of GAB Eq. (3), for $K = 1$, and is more appropriate for RH values between 5% and 40%.
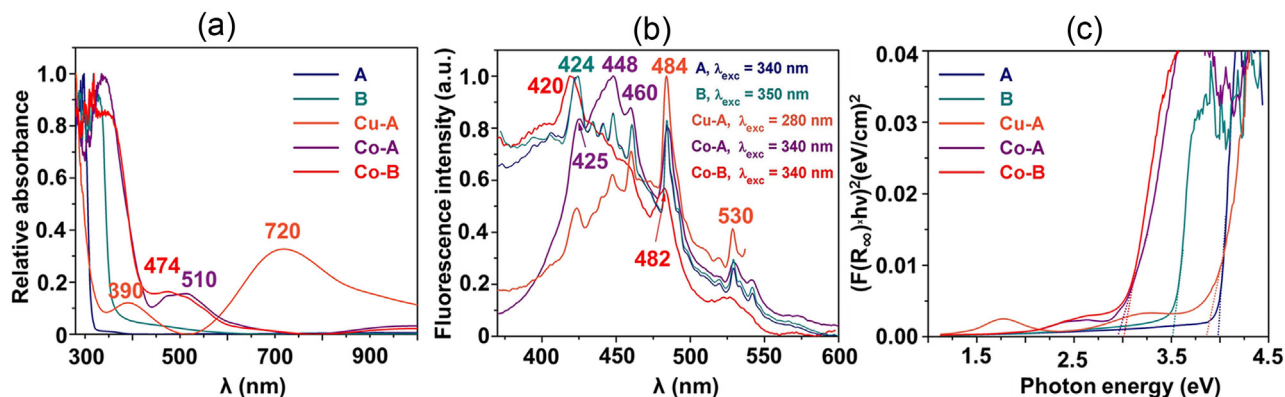
Fig. 6. Spectral characteristics of the ligands and complexes: (a) Normalized diffuse reflectance spectra; (b) normalized fluorescence spectra; (c) the Tauc plot of $[F(R_\infty) \times h\nu]^2$ vs. photon energy.

The GAB equation is used for a larger domain of relative humidity between 5% and 90% [83]. Both models were applied on the desorption branch of the isotherms. BET and GAB models are used for finding out the weight of water forming a monolayer and the surface area values, applying Eq. (4). Starting from the specific surface area, calculated from BET equation (A), the average pore size (r_{pm}) of materials was estimated, assuming cylindrical pore geometry and using Eq. (5) [84]:

$$A = \frac{W_m \cdot N_A \cdot 1.091 \cdot (M \cdot 10^{24}/\rho_a \cdot N_A)^{2/3}}{M} \quad (4)$$

Where: N_A-Avogadro's number ($6.022 \cdot 10^{23}$ mol^{-1}), M- molar mass of the adsorbate and ρ_a is the adsorbed phase density

$$r_{pm} = \frac{2 \cdot W}{100 \cdot \rho_a \cdot A} \quad (5)$$

In our case the BET model fitted better the registered data, but the values obtained from both methods were in good correlation. For the Co and Cu complexes, the pore size increased in the order: Co-A< Co-B <Cu-A. The highest surface area was found for Co-A.

3.1.6. UV–vis diffuse reflectance and photoluminescence

As observed in Fig. 6 from the DRS spectra, both ligands absorb especially in the UV region, due to the aromatic π-π* transition. The absorption edge for visible light of the ligands falls near 400 nm. Coordination with metallic ions enhanced the intensity by several times and displaced the absorption edge to the red. The complex of ligand A with Cu(II) ions present a weak band at 390 nm and a very strong band centered on 720 nm, assigned to the d–d transitions in the complex. The absorption edge of Cu-A is around 1060 nm. The two Co(II) complexes have the main band located between 450 and 600 nm and the absorption edge shifted to 700 nm. It appears that the spectral profiles of Co-A and Co-B are quite insensitive to introducing an ethynyl bridge between the two pyridyl rings.

The fluorescence emission was observed to be very strong for ligands and for complexes as well (Fig. 6b), but the profiles suggest the emission is ligand centered. The vibronic structure characteristic to the A and B ligands, associated with isolated chromophores and distinct emissions in the —CH$_2$—Si—O—Si—CH$_2$— frame, was not completely retained in the complexes. The differences in the metal center on the electronic distribution when A ligand is used is observed by the decreased intensity of the 448 nm band for Cu-A, probably given by some interstitial defects, and the massive increase of the blue emission at 484 nm. The last one altogether with the green band at 530 nm may be related to the electron-hole recombination of localized excitons and to some surface defects of the crystals [85,86]. Increased PL intensity of the specific band

for Cu-A would indicate a higher recombination rate of the photo-generated electrons and holes, leading to decrease of the catalytic performance [37]. For Co-B, containing the EBPy unit, the fine structure is almost gone and this can be interpreted as a substantial interaction between the chromophoric units in direct relationship with the flexibility of the pyridyl-ethylene linker. The high intensity and the hypsochromic displacement of the deep violettish-blue emission at 420 nm may indicate a higher degree of crystallinity as compared to the ligand and to the other two complexes.

The optical band gap of the ligands and their metal complexes was estimated from the DRS spectra in the Kubelka − Munk expression and according to the Tauc approach for a direct band gap [87]. Regardless the metal ion center, the E_g values lowered from ligands to complexes, a phenomenon assigned to a decreased energy at the organic linker − metallic ion or cluster interface due to charge redistribution between the two fragments [88]. Thus, the energy band gap decreased from 3.98 eV in A to 3.86 eV in Cu-A and to 2.95 eV in Co-A, while for the ligand B, the decrease is from 3.51 eV in B to 3.01 eV in Co-B. So, the Co complexes have similar energy band gap values, which are significantly narrower than that of the Cu complex.

3.2. Hydrogen peroxide decomposition with siloxane MOFs as catalysts

We focused on testing these metal complexes as catalysts, for two different applications, of practical importance. First, the catalytic activity for hydrogen peroxide decomposition in alkaline medium was evaluated as described previously [73], with similar amounts of catalyst. The conversion versus time (expressed as volume of evolved O$_2$ reported to the theoretical volume, per gram of catalyst) is plotted in Fig. 7a) for the three complexes and the previously reported Zn MOF obtained with the same ligands [73]. In the tested conditions, the best catalyst for hydrogen peroxide decomposition was Co-A, which allowed ca. 90% conversion after 30 min, followed by Co-B. The Cu complex allowed around 30% conversion in the same conditions. The effect of Co ions in alkaline hydrogen peroxide decomposition is long known [77] in cobalt-iron spinel oxides and it was explained by the surface oxidation of Co(II).

It is also known that this reaction is a first-order one. Thus, a plot of ln(C/C$_0$) (where C is the concentration of H$_2$O$_2$–calculated from the volume of O$_2$, C$_0$ the initial concentration) versus time gave the rate constants (k, s^{-1}) as the slope of the straight lines obtained for the first 800 s (Fig. 7b, Table 2). In order to compare with literature data, k values were expressed per catalyst mass unit. The values for the Co complexes are twice or three-fold higher than those reported for cobalt-iron oxides [77], while the Cu catalyst
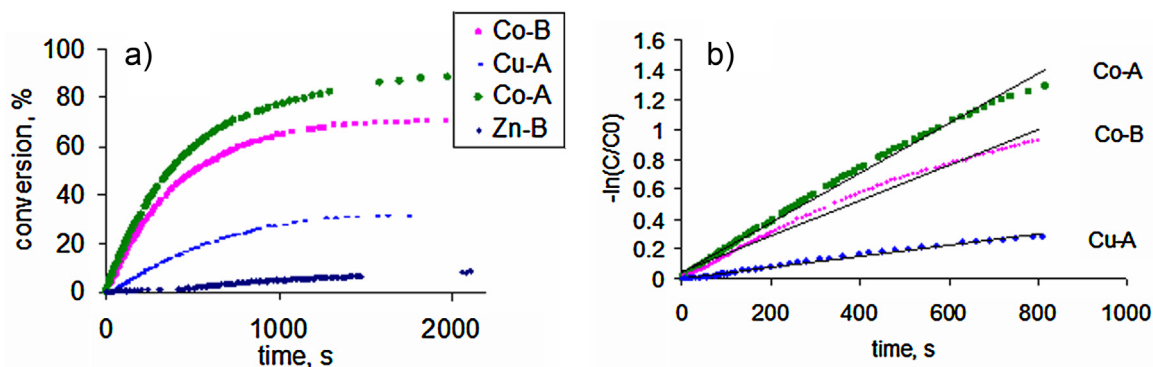
Fig. 7. a) Evolution of hydrogen peroxide decomposition in alkaline conditions, with MOFs as catalysts. For comparison, we used a MOF with Zn, obtained with the same ligands (Zn-B = polymer "IV" in our previous publication [73]); b) kinetics of hydrogen peroxide decomposition catalyzed by different metal complexes.

Table 2
Reaction rate parameters for the alkaline decomposition of H_2O_2 in the presence of metal complexes.

Sample	k, s^{-1}	R^2	k', $s^{-1} g^{-1}$
Co-A	0.0017	0.9942	0.68
Co-B	0.0012	0.9862	0.5
Cu-A	0.0004	0.9918	0.2

gave similar rate constant as the best oxide tested in this reference. The better catalytic activity of the MOFs compared to the oxides may be due to their ability to keep a flexible coordination sphere, which allows them a better reactivity as well as reactant shape selectivity [89].

It is interesting to note that the catalytic activity of the three complexes follows the reverse order of the pore size, estimated from DVS in water vapors sorption curves. The best catalyst (Co-A) has the smallest pore size and at the same time the highest surface area. On the other hand, given the fact that the reaction occurs in ambiental conditions, under natural light, this is a photochemical process. The efficiency of the catalysts reflects the reverse order of the energy band gap.

This system can be further used as oxidation medium for example of alcohols or biopolymers. The oxidation of cellulose and other biopolymers under mild conditions is a very actual research topic, since oxidized cellulose has important benefits, especially as biomaterial for medical use. On the other hand, the biggest challenge is to limit the fragmentation side reactions. Thus, oxidation of biopolymers is one very important possible application of the MOFs, since they are active in mild conditions. This subject is currently under investigation. As preliminary results, the model oxidation of cyclohexanol to cyclohexanone was carried out with H_2O_2 in acetonitrile, without addition of basic medium, using Co-A as catalyst at 35 °C for 1.5 h. The reaction medium was analyzed by ESI–MS. Cyclohexanone was detected as the main species, while cyclohexanol was not present in the spectrum (Fig. 5S), which is a promising result according to the literature [90]. The FT-IR and H NMR spectra also confirmed the reaction.

3.3. Photodecomposition of Congo red

Congo Red (CR) is an anionic diazo dye, with a high affinity for cellulose, thus it is used in textile industry. However, its high toxicity is one reason for limited use in modern days [91]. The removal of CR from residual waters is thus an important environmental issue. The characteristic UV–vis absorption spectrum of CR contains three absorption maxima, at 495 nm due to the azo chromophore, 343 nm and 237 nm, attributed to naphthalene and benzene rings, respectively [92].

3.3.1. Comparison between samples and some mechanism considerations

The photocatalytic degradation of CR was tested in the presence of the metal complexes under natural sunlight, without pH adjustments or artificial irradiation. In Fig. 6S, the absorption spectra of the Congo Red solutions after 80 min in the presence of all the metal complexes are represented for comparison. It is obvious that the absorption band at around 495 nm suffered a pronounced decrease in all cases and almost disappeared with Co-B catalyst. Also, one can observe the similarity of the spectra obtained in the presence of both Co catalysts, as opposed to a different shape of the electronic spectrum of the photodegradation product in the presence of Cu-A. The relative intensity of the absorption bands at 344 (I_1) and 496 nm (I_2) in the initial sample ($I_1/I_2 = 0.81$) increased after photodegradation, with some notable differences depending on the catalyst used. For the Cu based catalyst, a bathochromic shift of both bands (to 360 nm and 500 nm) was observed, as well as a pronounced decrease of the azo- band, while the intensity of the band at 360 nm was almost unchanged as compared to the pristine sample (the ratio of the absorbances was 1.96). In the case of Co catalysts, the band at 345 nm is overlapped after reaction; the estimated I_1/I_2 values were around 1.55, showing that the azo band was reduced in a higher extent than the aromatic band. Thus it is possible that different degradation mechanisms might apply depending on catalyst.

In order to test the dye adsorption, the CR solution with the catalyst was kept in the dark and the UV–vis spectra were followed for 2 h. In the hypothesis of preponderant adsorption phenomenon, both bands should have been modified proportionally, i.e. the absorbance intensity ratio should have been preserved [93]. The experiment with Cu-A gave practically unchanged spectrum (Fig. 7S a), while with Co-A it was impossible to avoid photodecomposition in spite of very quick manipulation and to discern between photodecomposition and possible adsorption. The modification of the azo band was more pronounced and the spectrum after ~50 min under dark was superimposed with that registered after exposure to sunlight for 20 min (Fig. 7S b). In addition, no mass modification of the catalyst was detected after immersion in dye solution for 1 h under dark. Also, the FT-IR spectrum of the catalyst after this experiment was unchanged. Thus we concluded that no significant physical adsorption occurs. This behavior could be explained by the hydrophobic nature of our MOFs, as was emphasized by the very low water sorption capacity measured by DVS, and lower surface area as compared with other materials.

According to most authors, the photodecomposition mechanism involves adsorption of the dye on the catalyst (which is usually hydrophilic and with high surface area) as the main or a preliminary step [53,94]. In our case, the contact of the catalyst with
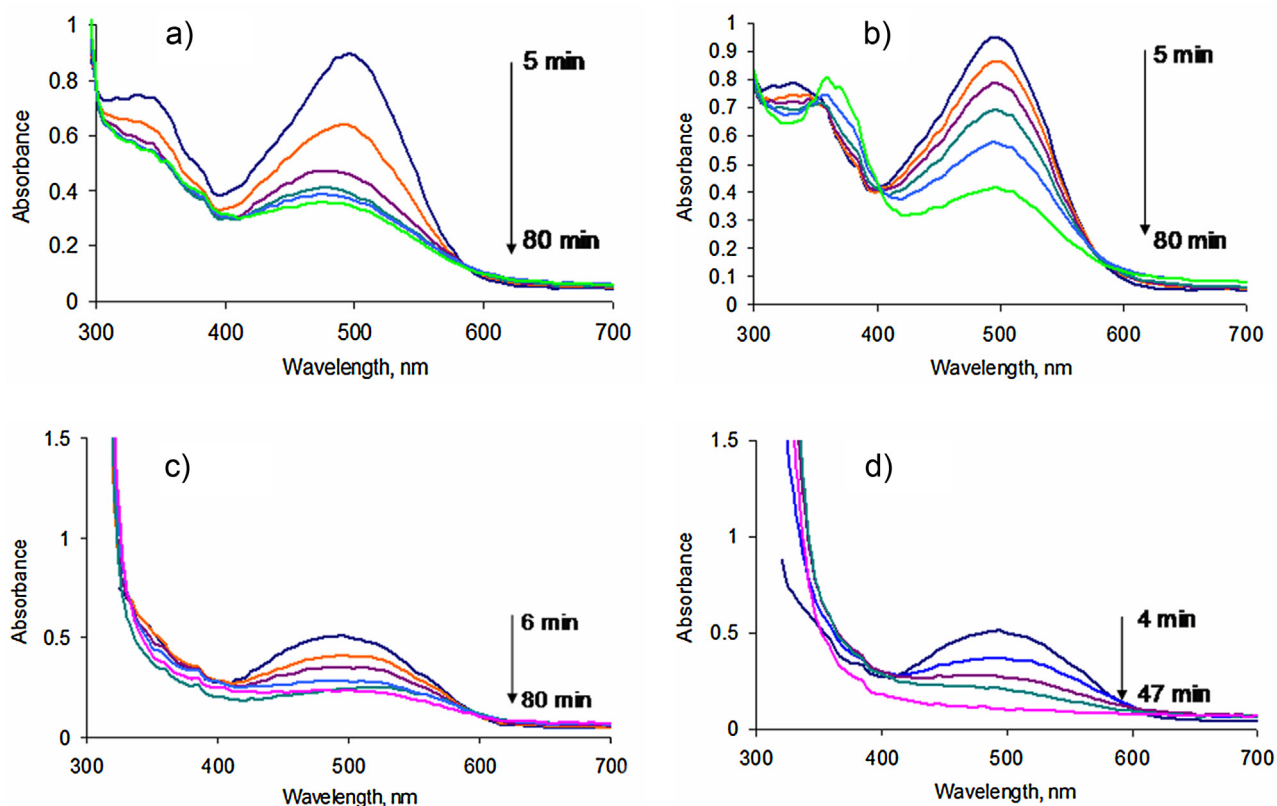
Fig. 8. The evolution of the UV–vis spectra of Congo Red solution in time, in the presence of different metal complexes as heterogeneous catalysts: Co-A (a), Cu-A (b), Co-B (c), and [Co-B + H$_2$O$_2$].

the dye aqueous solution is superficial and brief, and it probably initiates the photodecomposition, generating radicals which then propagate the process within the entire volume of the solution. The main active species generally accepted in this kind of reaction are: oxygen ion radical (O$_2^{\bullet-}$) and the hydroxyl radical (HO$^\bullet$), which are generated by the electrons and holes resulted in photoexcitation of the catalyst.

The exact mechanism in presence of each of these catalysts is challenging and deserves special attention in a future work. In the meanwhile, we evaluated comparatively the behavior of Co-B catalyst under ambient light, after purging the solution with argon (Fig. 8S). After 1.5 h, practically no difference in color could be noticed between the oxygen depleted solution and the reference, although both suffered discoloration. Thus, we suppose that in this case, the most important active species would probably be the hydroxyl radical, but more thorough investigations are necessary.

3.3.2. Kinetics of the photodecomposition under sunlight

The evolution of the UV–vis spectra with time and the reaction kinetics are shown in Figs. 8 and 9, for all the catalysts and the combination of Co-B and H$_2$O$_2$. As photodegradation is a pseudo-first-order reaction [49], the plots of −ln(A/A$_0$) versus time gave the apparent rate constants (Fig. 9a), which are shown in Table 3 together with the fitting parameters.

The rate constants obtained with the siloxane-containing MOFs alone were similar with those reported for ZnO@γ − Fe$_2$O$_3$ nanocomposites [49], used in similar dye/catalyst mass ratio, and are slightly lower than those reported for the same dye concentration, for an experiment conducted in a photoreactor using a WO$_3$–TiO$_2$/AC (activated carbon) and H$_2$O$_2$ catalytic system [95]. The effect of H$_2$O$_2$ addition was a significant speed up of the discoloration process, the reaction rate being more than double in

Table 3
Apparent rate constants and fitting parameters for pseudo first-order photodegradation reaction of Congo Red in the presence of metal complexes as catalysts.

Metal complex	Rate constant (k), min^{-1}	R^2	Efficiency[b] after 80 min, %
Co-A	0.0163	0.915	68.1
Cu-A	0.0102	0.904	64
Co-B	0.0188[a]	0.833	81.6
Co-B + H$_2$O$_2$	0.0405	0.98	97

[a] The best fitting was obtained when two processes are considered: one in the first 6 min, with k1 = 0.1152 min^{-1} and the other with k2 = 0.0142 min^{-1} (R^2 = 0.91).
[b] The photocatalytic discoloration efficiency (color removal efficiency) was calculated as:
(A$_0$ − A)/A$_0$ × 100.

[Co-B + H$_2$O$_2$] system than the overall rate when Co-B was used alone. This is not surprising, since it is known that hydrogen peroxide enhances the degradation due to generation of hydroxyl radicals [96], while Co (II) in the MOF is oxidized, as suggested in the literature [56]. If hydrogen peroxide is added in our system, the rate constant significantly surpasses the ones previously reported [95], although in our case the irradiation source was natural light.

3.3.3. Color removal efficiency

The photocatalytic discoloration efficiency of CR (color removal efficiency) reached 81.6% after 80 min of exposure to sunlight, with Co-B as catalyst and 97% for [Co-B + H$_2$O$_2$] Fenton-like process (Fig. 9b). Since the efficiency of the catalyst Co-B alone was very high within observation time, the use of H$_2$O$_2$ might not be absolutely necessary. Co-B catalyst exhibited a particular behavior, with a very fast reaction step within the first few minutes followed by a slower process. Its efficiency after only 6 min in the sunlight reached 50%, which to our knowledge, is the best result reported so
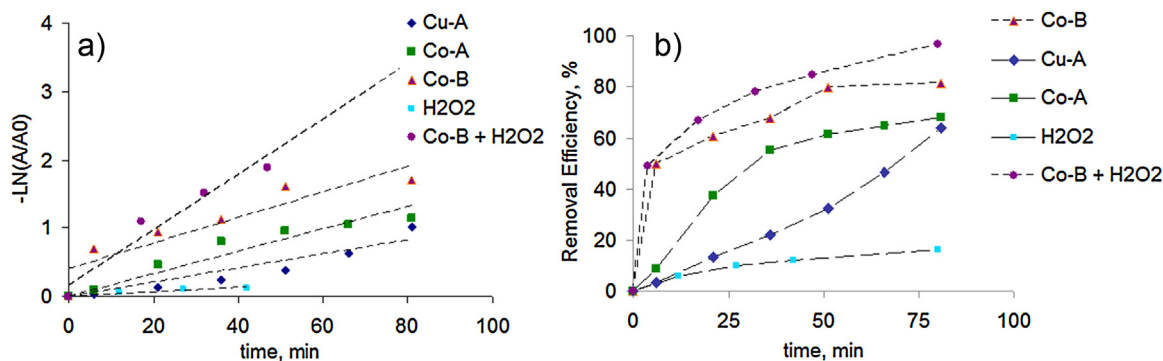
Fig. 9. The −ln(A/A$_0$) vs. time plot used for determining pseudo-first-order reaction rate constants (a) and the discoloration efficiency (b).
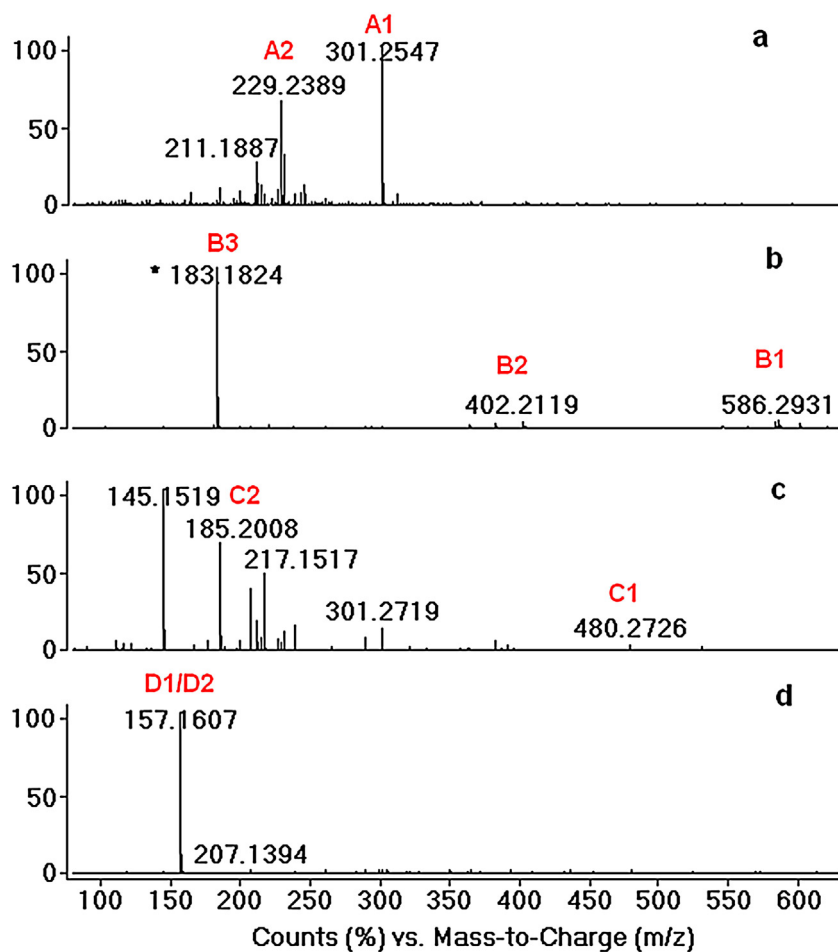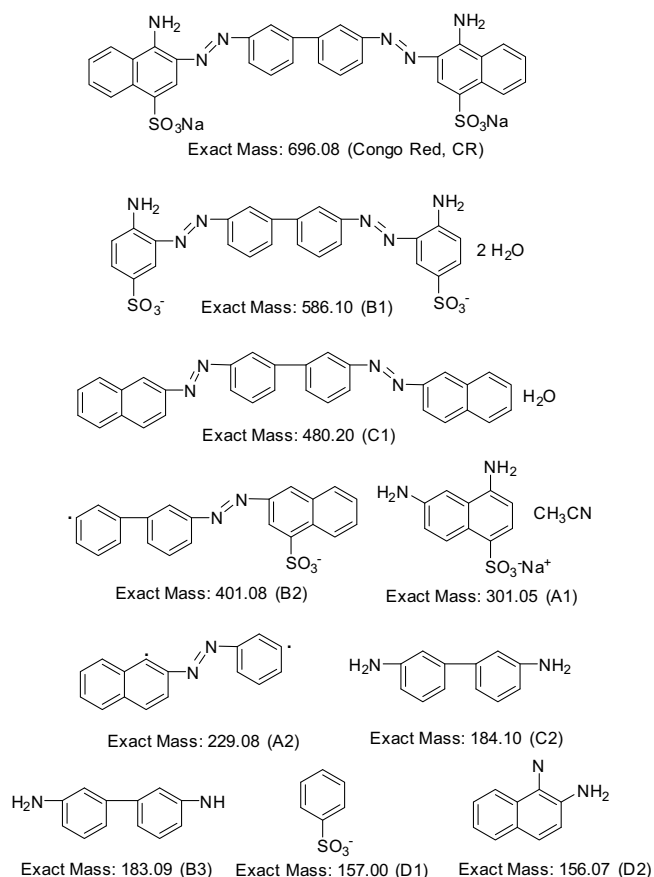

Fig. 10. Positive ESI mass spectra of discolored CR solutions in water- acetonitrile solutions 9:1 (v/v): a) only H2O2 as catalyst; b) Co-B catalyst; c) [Co-B+H2O2] system; d) Cu-A catalyst.

far. Even when the CR solution with Co-B was not exposed to direct sunlight but in ambiental light or even in the dark, the discoloration was obvious within short time (Fig. 8S). It is worth mentioning that all the solutions became colorless after longer time, varying from several hours to several days of storing in the laboratory (with no direct exposure to sunlight), depending on the catalyst and most probably on light intensity.

The better catalytic activity in terms of degradation efficiency and rate constant found for the Co complexes is in agreement with the lower energy band gap, as compared to Cu catalyst. Catalytic activity in reverse order with respect to the band gap values is usually observed [53].

The general trend of the photodegradation process was similar during various tests conducted in different days. It is worth mentioning that all the metal complexes acted as heterogeneous catalysts, being insoluble and hardly dispersible in water. Neither permanent stirring, nor sonication was applied for increased dispersion of the catalysts in our small scale testing; the recipients containing the solution and the catalysts were manually shacked before each exposure to sunlight. At the end of the process, the catalyst and the eventually formed precipitate were removed by simple filtration. The filtrated water was analyzed by XRF and no trace of metal was detected (Fig. 9S).

Scheme 2. Chemical structure and exact mass of Congo Red (CR) and possible degradation compounds as fragments detected by ESI–MS in the filtered solutions.

3.3.4. MS analysis of the purified water

In order to determine the degradation products of Congo Red remained in water after treatment with MOFs catalysts and filtration, ESI–MS analysis was performed (acetonitrile was added for analysis, water/acetonitrile 9:1 (v/v)). The formation of the molecular ion by ESI–MS occurs in positive mode and therefore only positive ions were analysed. The ESI–MS spectra for the photodegradation products of CR after reaction with H_2O_2, Co-B, [Co-B +H_2O_2] and Cu-A are shown in Fig. 10. The species detected in solution after discoloration were assigned according to Scheme 2 and were partly recognised by other authors [39]. It is obvious that unchanged CR was not detected. In the sample treated with H_2O_2, the highest mass detected was at $m/z = 301.25$, which most probably corresponds to structure "A1". The peak at $m/z = 229.24$ could be assigned to structure "A2", which is the smallest fragment containing azo group. In all spectra of the MOF catalyzed reactions, only traces of azo- containing compounds were detected (for example structures B1, B2, C1), while most of the detected species were low molecular weight fragments (B3, C2, D1 or D2) or even inorganic compounds ($m/z = 145.15$ in Fig. 10c is probably Na_2SO_3).

As an overall aspect, the experiments carried out with Co-B (Fig. 10b) or Cu-A (Fig. 10d), without additional H_2O_2 gave "cleaner" spectra than those obtained with H_2O_2. This is consistent with the largely accepted oxidation mechanism, which involves higher level of radical species when H_2O_2 is used [60,61], generating more by-products. On the other hand, the very low amount of large organic species detected in the mass spectra indicates improved quality of the wastewaters after treatment with the MOFs alone.

In terms of environmental impact, the wastewaters treatment under natural sunlight is much more efficient, with no artificial energy input. Moreover, the synthesis of these catalysts implies minimal energy consumption compared with other catalytic systems, which makes the overall process very effective.

4. Conclusions

Three new MOFs were obtained from a siloxane dicarboxylic acid (CX), 4,4′-bipyridyne (BPy) or 1,2-bis(4-pyridyl)ethylene (EBPy) and copper or cobalt acetates, at room temperature, in DMF. The compounds were tested as catalysts in alkaline decomposition of hydrogen peroxide and in photodecomposition of Congo Red (CR) under sunlight, in ambient conditions.

Very good catalytic performance was obtained especially for the Co complexes. The best conversion in H_2O_2 decomposition was ca. 90% after 30 min with the compound having the smallest pore size, the highest surface area and the lowest energy band gap. The reactions followed first order kinetics, with rate constants better than those reported in similar conditions for Co-Fe oxides.

The catalytic activity in photodecomposition of Congo Red (CR) was successfully tested in environmental conditions, i.e. under natural light, without additional oxidation agents or pH adjustments. Unprecedented catalytic activity was found, with discoloration efficiency of ca. 82% after 80 min of exposure to sunlight, and 50% discoloration after 6 min with the Co complex of CX and EBPy, which exhibited a particular behavior. The results obtained under mild, environmental conditions, were comparable in terms of rate constants and efficiency with those reported for other catalytic systems in photoreactors or in the presence of H_2O_2 as oxidation agent.

The addition of H_2O_2 in a Fenton-like process doubles the rate constant and increases the efficiency to 97%. The remaining waters after CR photodecomposition and filtration were analyzed by XRF and no metal trace was detected. By mass spectrometry (ESI–MS) it was found that the MOFs alone can yield cleaner water as compared with the case when H_2O_2 was used. Thus the photodecomposi-

The reuse of the catalysts is possible in principle, as we observed in qualitative experiments. Since we used natural sunlight, the precise quantification of multiple use efficiency could be susceptible to approximation. However, comparing the FT-IR spectra of Co-B before and after use in CR photodegradation, it was obvious that its structure was preserved (Fig. 10S). The natural light as photoirradiation source might be regarded as a disadvantage from fundamental point of view, since the light intensity is not constant. In fact, this only limits our knowledge on the highest possible performance in specific conditions, but it does not change the essential findings, that these compounds act as very effective catalysts, alone or in combination with hydrogen peroxide, and that they can ultimately lead to total discoloration of CR solution.

The high degradation efficiency found under natural visible light irradiation is an outstanding result for MOFs. High removal efficiency of over 90% are generally obtained in Fenton-like processes [58,60], while lower values were reported for heterogeneous systems without additional oxidation agent [59]. Also, the source of irradiation has a great relevance when comparing different reported results, since in most cases an UV lamp is used for irradiation. The best removal efficiency reported so far for CR with MOFs without auxiliary oxidants (94%) was obtained after 120 min under artificial UV irradiation [59], while with visible light it didn't exceed 50% within the same timeframe, which makes our compounds very attractive (for example, as mentioned above, 50% discoloration can be achieved with Co-B within 5–6 min with no significant influence of the sunlight intensity).

tion of CR may be successfully conducted without oxidation agents, although it requires longer time, since total discoloration occurs even in ambiental light. The catalysts can be removed by filtration and re-used, since they preserve their structure. According to our knowledge, this is the first example of a hydrophobic MOF acting as efficient photocatalyst in water.

Appendix A. Supplementary data

Supplementary data associated with this article can be found, in the online version, at http://dx.doi.org/10.1016/j.apcatb.2016.12.034.

References

[1] M. Peplow, Materials science: the hole story, Nature 520 (2015) 148–150, http://dx.doi.org/10.1038/520148a.

[2] J.J. Perry IV, J.A. Perman, M.J. Zaworotko, Design and synthesis of metal-organic frameworks using metal-organic polyhedra as supermolecular building blocks, Chem. Soc. Rev. 38 (2009) 1400–1417, http://dx.doi.org/10.1039/b807086p.

[3] D. Zhao, D.J. Timmons, D. Yuan, H.-C. Zhou, Tuning the topology and functionality of metal–organic frameworks by ligand design, Acc. Chem. Res. 44 (2011) 123–133, http://dx.doi.org/10.1021/ar100112y.

[4] S.L. James, Metal-organic frameworks, Chem. Soc. Rev. 32 (2003) 276–288, http://dx.doi.org/10.1039/B200393G.

[5] D.J. Tranchemontagne, J.L. Mendoza-Cortés, M. O'Keeffe, O.M. Yaghi, Secondary building units, nets and bonding in the chemistry of metal-organic frameworks, Chem. Soc. Rev. 38 (2009) 1257–1283, http://dx.doi.org/10.1039/b817735j.

[6] L.J. Murray, M. Dincă, J.R. Long, Hydrogen storage in metal-organic frameworks, Chem. Soc. Rev. 38 (2009) 1294–1314, http://dx.doi.org/10.1039/b802256a.

[7] S.S. Han, J.L. Mendoza-Cortés, W.A. Goddard III, Recent advances on simulation and theory of hydrogen storage in metal-organic frameworks and covalent organic frameworks, Chem. Soc. Rev. 38 (2009) 1460–1476, http://dx.doi.org/10.1039/b802430éh.

[8] D.J. Collins, H.-C. Zhou, Hydrogen storage in metal-organic frameworks, J. Mater. Chem. 17 (2007) 3154–3160, http://dx.doi.org/10.1039/b702858j.

[9] Z. Hulvey, E.H.L. Falcao, J. Eckert, A.K. Cheetham, Enhanced H_2 adsorption enthalpy in the low-surface area, partially fluorinated coordination polymer $Zn_5(triazole)_6(tetrafluoroterephthalate)_2(H_2O)_2 \cdot 4H_2O$, J. Mater. Chem. 19 (2009) 4307–4309, http://dx.doi.org/10.1039/b900879a.

[10] Antek G. Wong-Foy, Adam J. Matzger, Omar M. Yaghi, Exceptional H2 saturation uptake in microporous metal–organic frameworks, J. Am. Chem. Soc. 128 (2006) 3494–3495, http://dx.doi.org/10.1021/JA058213H.

[11] X. Lin, J. Jia, P. Hubberstey, M. Schröder, N.R. Champness, Hydrogen storage in metal–organic frameworks, CrystEngComm 9 (2007) 438–448, http://dx.doi.org/10.1039/B706207A.

[12] R.B. Getman, Y.-S. Bae, C.E. Wilmer, R.Q. Snurr, Review and analysis of molecular simulations of methane, hydrogen, and acetylene storage in metal–organic frameworks, Chem. Rev. 112 (2012) 703–723, http://dx.doi.org/10.1021/cr200217c.

[13] J.-R. Li, R.J. Kuppler, H.-C. Zhou, Selective gas adsorption and separation in metal–organic frameworks, Chem. Soc. Rev. 38 (2009) 1477–1504, http://dx.doi.org/10.1039/b802426j.

[14] T. Düren, Y.-S. Bae, R.Q. Snurr, Using molecular simulation to characterise metal–organic frameworks for adsorption applications, Chem. Soc. Rev. 38 (2009) 1237–1247, http://dx.doi.org/10.1039/b803498m.

[15] M. Kondo, T. Yoshitomi, H. Matsuzaka, S. Kitagawa, K. Seki, Three-dimensional framework with channeling cavities for small molecules: {[M2(4, 4′-bpy)3(NO3)4]·xH2O}n (M = Co, Ni, Zn), Angew. Chemie Int. Ed. Engl. 36 (1997) 1725–1727, http://dx.doi.org/10.1002/anie.199717251.

[16] K. Sumida, D.L. Rogow, J.A. Mason, T.M. McDonald, E.D. Bloch, Z.R. Herm, T.-H. Bae, J.R. Long, Carbon dioxide capture in metal–organic frameworks, Chem. Rev. 112 (2012) 724–781, http://dx.doi.org/10.1021/cr2003272.

[17] H. Wu, Q. Gong, D.H. Olson, J. Li, Commensurate adsorption of hydrocarbons and alcohols in microporous metal organic frameworks, Chem. Rev. 112 (2012) 836–868, http://dx.doi.org/10.1021/cr200216x.

[18] J.-R. Li, J. Sculley, H.-C. Zhou, metal–organic frameworks for separations, Chem. Rev. 112 (2012) 869–932, http://dx.doi.org/10.1021/cr200190s.

[19] M.D. Allendorf, C.A. Bauer, R.K. Bhakta, R.J.T. Houk, Luminescent metal–organic frameworks, Chem. Soc. Rev. 38 (2009) 1330–1352, http://dx.doi.org/10.1039/b802352m.

[20] L.E. Kreno, K. Leong, O.K. Farha, M. Allendorf, R.P. Van Duyne, J.T. Hupp, Metal–organic framework materials as chemical sensors, Chem. Rev. 112 (2012) 1105–1125, http://dx.doi.org/10.1021/cr200324t.

[21] A. Bétard, R.A. Fischer, Metal–organic framework thin films: from fundamentals to applications, Chem. Rev. 112 (2012) 1055–1083, http://dx.doi.org/10.1021/cr200167v.

[22] J. Lee, O.K. Farha, J. Roberts, K.A. Scheidt, S.T. Nguyen, J.T. Hupp, Metal–organic framework materials as catalysts, Chem. Soc. Rev. 38 (2009) 1450–1459, http://dx.doi.org/10.1039/b807080f.

[23] L. Ma, C. Abney, W. Lin, Enantioselective catalysis with homochiral metal–organic frameworks, Chem. Soc. Rev 38 (2009) 1248–1256, http://dx.doi.org/10.1039/b807083k.

[24] T. Uemura, N. Yanai, S. Kitagawa, Polymerization reactions in porous coordination polymers, Chem. Soc. Rev. 38 (2009) 1228–1236, http://dx.doi.org/10.1039/b802583p.

[25] A. Corma, H. Garciía, F.X. Llabreís i Xamena, Engineering metal organic frameworks for heterogeneous catalysis, Chem. Rev. 110 (2010) 4606–4655, http://dx.doi.org/10.1021/cr9003924.

[26] M. Kurmoo, Magnetic metal–organic frameworks, Chem. Soc. Rev. 38 (2009) 1353–1379, http://dx.doi.org/10.1039/b804757j.

[27] Z. Ming-Hua, W. Bo, W. Xin-Yi, Z. Wei-Xiong, C. Xiao-Ming, G. Song, Chiral magnetic metal-organic frameworks of dimetal subunits: magnetism tuning by mixed-metal compositions of the solid solutions, Inorg. Chem. 45 (2006) 7069–7076, http://dx.doi.org/10.1021/IC060520G.

[28] C. Wang, T. Zhang, W. Lin, Rational synthesis of noncentrosymmetric Metal–Organic frameworks for second-order nonlinear optics, Chem. Rev. 112 (2012) 1084–1104, http://dx.doi.org/10.1021/cr200252n.

[29] S. Loera-Serna, E. Ortiz, Catalytic applications of metal-organic frameworks, in: L.E. Norena, J.-A. Wang (Eds.), Advanced Catalytic Materials—Photocatalysis and Other Current Trends, InTech, 2016, http://dx.doi.org/10.5772/61865.

[30] D. Farrusseng, S. Aguado, C. Pinel, Metal-organic frameworks opportunities for catalysis, Angew. Chemie Int Ed. 48 (2009) 7502–7513, http://dx.doi.org/10.1002/anie.200806063.

[31] J. Gascon, A. Corma, F. Kapteijn, F.X. Llabrés i Xamena, Metal organic framework catalysis: Quo vadis? ACS Catal. 4 (2014) 361–378, http://dx.doi.org/10.1021/cs400959k.

[32] K. Leus, Y.-Y. Liu, P. Van Der Voort, Metal-organic frameworks as selective or chiral oxidation catalysts, Catal. Rev. 56 (2014) 1–56, http://dx.doi.org/10.1080/01614940.2014.864145.

[33] M. Ranocchiari, J.A. van Bokhoven, Catalysis by metal–organic frameworks: fundamentals and opportunities, Phys. Chem. Phys. 13 (2011) 6388–6396, http://dx.doi.org/10.1039/c0cp02394a.

[34] A.H. Chughtai, N. Ahmad, H.A. Younus, A. Laypkov, F. Verpoort, Metal–organic frameworks: versatile heterogeneous catalysts for efficient catalytic organic transformations, Chem. Soc. Rev. 44 (2015) 6804–6849, http://dx.doi.org/10.1039/C4CS00395K.

[35] V.I. Isaeva, L.M. Kustov, The application of metal-organic frameworks in catalysis (Review), Pet. Chem. 50 (2010) 167–180, http://dx.doi.org/10.1134/S0965544110030011.

[36] H. Wang, X. Yuan, Y. Wu, G. Zeng, H. Dong, X. Chen, L. Leng, Z. Wu, L. Peng, In situ synthesis of In2S3@MIL-125(Ti) core–shell microparticle for the removal of tetracycline from wastewater by integrated adsorption and visible-light-driven photocatalysis, Appl. Catal. B Environ. 186 (2016) 19–29, http://dx.doi.org/10.1016/j.apcatb.2015.12.041.

[37] H. Wang, X. Yuan, Y. Wu, G. Zeng, X. Chen, L. Leng, H. Li, Synthesis and applications of novel graphitic carbon nitride/metal-organic frameworks mesoporous photocatalyst for dyes removal, Appl. Catal. B Environ. 174 (2015) 445–454, http://dx.doi.org/10.1016/j.apcatb.2015.03.037.

[38] M. Bagheri, A.R. Mahjoub, B. Mehri, Enhanced photocatalytic degradation of Congo Red by solvothermally synthesized CuInSe₂–ZnO nanocomposites, RSC Adv. 4 (2014) 21757–21764, http://dx.doi.org/10.1039/c4ra01753f.

[39] S. Erdemoğlu, S.K. Aksu, F. Sayılkan, B. İzgi, M. Asiltürk, H. Sayılkan, F. Frimmel, Ş. Güçer, Photocatalytic degradation of Congo Red by hydrothermally synthesized nanocrystalline TiO2 and identification of degradation products by LC–MS, J. Hazard. Mater. 155 (2008) 469–476, http://dx.doi.org/10.1016/j.jhazmat.2007.11.087.

[40] M. Pelaez, N.T. Nolan, S.C. Pillai, M.K. Seery, P. Falaras, A.G. Kontos, P.S.M. Dunlop, J.W.J. Hamilton, J.A. Byrne, K. O'shea, M.H. Entezari, D.D. Dionysiou, A review on the visible light active titanium dioxide photocatalysts for environmental applications, Appl. Catal. B Environ. 125 (2012) 331–349, http://dx.doi.org/10.1016/j.apcatb.2012.05.036.

[41] C.E. Bonancêa, G.M. do Nascimento, M.L. de Souza, M.L.A. Temperini, P. Corio, Substrate development for surface-enhanced Raman study of photocatalytic degradation processes: congo red over silver modified titanium dioxide films, Appl. Catal. B Environ. 69 (2006) 34–42, http://dx.doi.org/10.1016/j.apcatb.2006.05.016.

[42] J. Wang, Y. Jiang, Z. Zhang, G. Zhao, G. Zhang, T. Ma, W. Sun, Investigation on the sonocatalytic degradation of Congo red catalyzed by nanometer rutile TiO2 powder and various influencing factors, Desalination 216 (2007) 196–208, http://dx.doi.org/10.1016/j.desal.2006.11.024.

[43] H. Zhu, R. Jiang, L. Xiao, Y. Chang, Y. Guan, X. Li, G. Zeng, Photocatalytic decolorization and degradation of Congo red on innovative crosslinked chitosan/nano-CdS composite catalyst under visible light irradiation, J. Hazard. Mater. 169 (2009) 933–940, http://dx.doi.org/10.1016/j.jhazmat.2009.04.037.

[44] E. uti, N. Laouedj, B. Ahmed, ZnO-assisted photocatalytic degradation of Congo red and benzopurpurine 4 B in aqueous solution, J. Chem. Eng. Process Technol. 2 (2011) 1000106, http://dx.doi.org/10.4172/2157-7048.1000106.

[45] M. Movahedi, A.R. Mahjoub, S. Janitabar-Darzi, Photodegradation of Congo Red in aqueous solution on ZnO as an alternative catalyst to TiO₂, J. Iran. Chem. Soc. 6 (2009) 570–577, http://dx.doi.org/10.1007/BF03246536.

[46] M. Shanthi, V. Kuzhalosai, Photocatalytic degradation of an azo dye, Acid Red 27, in aqueous solution using nano ZnO, Indian J. Chem. A 51A (2012) 428–434.

[47] H.R. Pouretedal, M.H. Keshavarz, Study of Congo Red photodegradation kinetic catalyzed by Zn1-XCuXS and Zn1-XNiXS nanoparticles, Int. J. Phys. Sci. 6 (2011) 6268–6279, http://dx.doi.org/10.5897/IJPS09.251.

[48] P. Samoila, C. Cojocaru, L. Sacarescu, P.P. Dorneanu, A.-A. Domocos, A. Rotaru, Remarkable catalytic properties of rare-earth doped nickel ferrites synthesized by sol-gel auto-combustion with maleic acid as fuel for CWPO of dyes, Appl. Catal. B Environ. 202 (2017) 21–32, http://dx.doi.org/10.1016/j.apcatb.2016.09.012.

[49] S.K. Yadav, P. Jeevanandam, Synthesis of ZnO@γ-Fe2O3 core–shell nanocomposites by a facile thermal decomposition approach and their application in photocatalytic degradation of Congo Red, J. Nanopart. Res. 18 (2016) 195, http://dx.doi.org/10.1007/s11051-016-3502-2.

[50] W.-S. Kuo, W.-Y. Chen, W.-S. Kuo, W.-Y. Chen, Solar Photocatalytic degradation of azo dye in aqueous TiO2 suspension assisted by Fresnel Lens, Int. J. Photoenergy. 2012 (2012) 1–7, http://dx.doi.org/10.1155/2012/303586.

[51] T. Erzsébet, W. László, P. Tamás, Azo dye degradation by high-energy irradiation: kinetics and mechanism of destruction, Nukleonika 52 (2007) 69–75.

[52] L. Ali, R. Algaithi, H.M. Habib, U. Souka, M.A. Rauf, S. Ashraf, Soybean peroxidase-mediated degradation of an azo dye?a detailed mechanistic study, BMC Biochem. 14 (2013) 35, http://dx.doi.org/10.1186/1471-2091-14-35.

[53] C.-C. Wang, J.-R. Li, X.-L. Lv, Y.-Q. Zhang, G. Guo, Photocatalytic organic pollutants degradation in metal?organic frameworks, Energy Environ. Sci. 7 (2014) 2831–2867, http://dx.doi.org/10.1039/C4EE01299B.

[54] Z.-Y. Gu, J. Park, A. Raiff, Z. Wei, H.-C. Zhou, Metal-organic frameworks as biomimetic catalysts, ChemCatChem 6 (2014) 67–75, http://dx.doi.org/10.1002/cctc.201300493.

[55] M. Partha, M. Giridhar, N. Srinivasan, Novel photocatalysts for the decomposition of organic dyes based on metal-organic framework compounds, J. Phys. Chem. B 110 (2006) 13759–13768, http://dx.doi.org/10.1021/JP0622381.

[56] M. Roy, S. Sengupta, S. Bala, S. Bhattacharya, R. Mondal, Systematic study of mutually inclusive influences of temperature and substitution on the coordination geometry of Co(II) in a series of coordination polymers and their properties, Cryst. Growth Des. 16 (2016) 3170–3179, http://dx.doi.org/10.1021/acs.cgd.5b01835.

[57] C.-L. Ming, H. Zhang, G.-Y. Li, G.-H. Cui, Assembly and catalytic properties of a 3D (4,6)-connected cobalt-organic framework with fsh topology, Bull. Korean Chem. Soc. 35 (2014) 651–654, http://dx.doi.org/10.5012/bkcs.2014.35.2.651.

[58] J.C. Geng, L.W. Liu, S.L. Xiao, G.H. Cui, Two 2D cobalt(II) coordination frameworks with unusual binodal network topology: synthesis, structures, and catalytic properties, Transit. Met. Chem. 38 (2013) 143–148, http://dx.doi.org/10.1007/s11243-012-9671-7.

[59] M.Y. Masoomi, M. Bagheri, A. Morsali, High efficiency of mechanosynthesized Zn-based metal–organic frameworks in photodegradation of Congo Red under UV and visible light, RSC Adv. 6 (2016) 13272–13277, http://dx.doi.org/10.1039/C5RA24238J.

[60] L. Qin, L. Liu, X. Du, G. Cui, Two dinuclear copper(II) complexes based on 5,6-dimethylbenzimidazole ligands: synthesis, crystal structures, and catalytic properties, Transit. Met. Chem. 38 (2013) 85–91, http://dx.doi.org/10.1007/s11243-012-9664-6.

[61] L. Qin, Y. Gu, G.Y. Li, S.L. Xiao, G.H. Cui, Preparation and crystal structure of a triple parallel interpenetrated copper coordination polymer based on a flexible bis(imidazole) ligand, Transit. Met. Chem. 38 (2013) 407–412, http://dx.doi.org/10.1007/s11243-013-9705-9.

[62] M. Du, C.-P. Li, C.-S. Liu, S.-M. Fang, Design and construction of coordination polymers with mixed-ligand synthetic strategy, Coord. Chem. Rev. 257 (2013) 1282–1305, http://dx.doi.org/10.1016/j.ccr.2012.10.002.

[63] A. Vlad, M. Cazacu, M.-F. Zaltariov, S. Shova, C. Turta, A. Airinei, Metallopolymeric structures containing highly flexible siloxane sequence, Polymer (Guildf) 54 (2013) 43–53, http://dx.doi.org/10.1016/j.polymer.2012.11.021.

[64] A. Vlad, M.-F. Zaltariov, S. Shova, G. Novitchi, C.-D. Varganici, C. Train, M. Cazacu, Flexible linkers and dinuclear metallic nodes build up an original metal–organic framework, CrystEngComm 15 (2013) 5368–5375, http://dx.doi.org/10.1039/c3ce40506k.

[65] M.-F. Zaltariov, A. Vlad, M. Cazacu, S. Shova, M. Balan, C. Racles, A Novel siloxane-containing dicarboxylic acid, 1,3-bis(p-carboxyphenylene-ester-methylene)tetramethyldisiloxane, and its derivatives: ester macrocycle and supramolecular structure with a copper complex, Tetrahedron 70 (2014) 2661–2668, http://dx.doi.org/10.1016/j.tet.2014.02.061.

[66] A. Vlad, M. Cazacu, M.-F. Zaltariov, A. Bargan, S. Shova, C. Turta, A 2D metal–organic framework based on dizinc coordination units bridged through both flexible and rigid ligands, J. Mol. Struct. 1060 (2014) 94–101, http://dx.doi.org/10.1016/j.molstruc.2013.12.029.

[67] S. Zuluaga, E.M.A. Fuentes-Fernandez, K. Tan, F. Xu, J. Li, Y.J. Chabal, T. Thonhauser, Understanding and controlling water stability of MOF-74, J. Mater. Chem. A 4 (2016) 5176–5183, http://dx.doi.org/10.1039/C5TA10416E.

[68] D. Ma, Y. Li, Z. Li, Tuning the moisture stability of metal–organic frameworks by incorporating hydrophobic functional groups at different positions of ligands, Chem. Commun. 47 (2011) 7377–7379, http://dx.doi.org/10.1039/c1cc11752a.

[69] D. Lombardo, M.A. Kiselev, S. Magazù, P. Calandra, Amphiphiles self-assembly: basic concepts and future perspectives of supramolecular approaches, adv, Condens. Matter Phys. 2015 (2015) 1–22, http://dx.doi.org/10.1155/2015/151683.

[70] A. Soroceanu, M. Cazacu, S. Shova, C. Turta, J. Kožíšek, M. Gall, M. Breza, P. Rapta, T.C.O. Mac Leod, A.J.L. Pombeiro, J. Telser, A.A. Dobrov, V.B. Arion, Copper(II) complexes with schiff bases containing a disiloxane unit: synthesis, structure, bonding features and catalytic activity for aerobic oxidation of benzyl alcohol, Eur. J. Inorg. Chem. 2013 (2013) 1458–1474, http://dx.doi.org/10.1002/ejic.201201080.

[71] M.-F. Zaltariov, M. Alexandru, M. Cazacu, S. Shova, G. Novitchi, C. Train, A. Dobrov, M.V. Kirillova, E.C.B.A. Alegria, A.J.L. Pombeiro, V.B. Arion, Tetranuclear Copper(II) complexes with macrocyclic and open-chain disiloxane ligands as catalyst precursors for hydrocarboxylation and oxidation of alkanes and 1-Phenylethanol, Eur. J. Inorg. Chem. 2014 (2014) 4946–4956, http://dx.doi.org/10.1002/ejic.201402578.

[72] M. Alexandru, M. Cazacu, A. Arvinte, S. Shova, C. Turta, B.C. Simionescu, A. Dobrov, E.C.B.A. Alegria, L.M.D.R.S. Martins, A.J.L. Pombeiro, V.B. Arion, μ-Chlorido-bridged Dimanganese(II) complexes of the schiff base derived from [2 + 2] condensation of 2,6-Diformyl-4-methylphenol and 1,3-Bis(3-aminopropyl)tetramethyldisiloxane: structure, magnetism, electrochemical behaviour, and catalytic oxidation of sec, Eur. J. Inorg. Chem. 2014 (2014) 120–131, http://dx.doi.org/10.1002/ejic.201300969.

[73] C. Racles, S. Shova, M. Cazacu, D. Timpu, New highly ordered hydrophobic siloxane-based coordination polymers, Polymer 54 (2013) 6096–6104, http://dx.doi.org/10.1016/j.polymer.2013.09.001.

[74] S.R. Collinson, W. Thielemans, The catalytic oxidation of biomass to new materials focusing on starch, cellulose and lignin, Coord. Chem. Rev. 254 (2010) 1854–1870, http://dx.doi.org/10.1016/j.ccr.2010.04.007.

[75] J.E. Mulvaney, C.S. Marvel, Disiloxane benzimidazole polymers, J. Polym. Sci. 50 (1961) 541–547, http://dx.doi.org/10.1002/pol.1961.1205015420.

[76] A. Dolgonos, T.O. Mason, K.R. Poeppelmeier, Direct optical band gap measurement in polycrystalline semiconductors: a critical look at the Tauc method, J. Solid State Chem. 240 (2016) 43–48, http://dx.doi.org/10.1016/j.jssc.2016.05.010.

[77] J.R. Goldstein, A.C.C. Tseung, The kinetics of hydrogen peroxide decomposition catalyzed by cobalt-iron oxides, J. Catal. 32 (1974) 452–465, http://dx.doi.org/10.1016/0021-9517(74)90096-7.

[78] K. Nakamoto, Infrared and Raman Spectra of Inorganic and Coordination Compounds, John Wiley & Sons, 1986, http://dx.doi.org/10.1021/ja00904a075.

[79] G. Socrates, Infrared and Raman Characteristic Group Frequencies: Tables and Charts, John Wiley & Sons, 2004.

[80] J.M. Seddon, Structural studies of liquid crystals by X-ray diffraction, in: D. Demus, J. Goodby, G.W. Gray, H.-W. Spiess, V. Vill (Eds.), Handb. Liq. Cryst. Set, Wiley-VCH Verlag GmbH, Weinheim, Germany, 1998, pp. 635–679, http://dx.doi.org/10.1002/9783527619276.

[81] E.S. Dragan, M. Cazacu, A. Nistor, Ionic organic/inorganic materials. III. Stimuli responsive hybrid hydrogels based on oligo(N, N –dimethylaminoethylmethacrylate) and chloroalkyl-functionalized siloxanes, J. Polym. Sci. Part A Polym. Chem. 47 (2009) 6801–6813, http://dx.doi.org/10.1002/pola.23720.

[82] C. Racles, A. Nistor, M. Cazacu, A silica-silver nanocomposite obtained by sol-gel method in the presence of silver nanoparticles, Cent. Eur. J. Chem. 11 (2013) 1689–1698, http://dx.doi.org/10.2478/s11532-013-0294-4.

[83] S. Brunauer, P.H. Emmett, E. Teller, Adsorption of gases in multimolecular layers, J. Am. Chem. Soc. 60 (1938) 309–319, http://dx.doi.org/10.1021/ja01269a023.

[84] K.L. Murray, N.A. Seaton, M.A. Day, An adsorption-based method for the characterization of pore networks containing both mesopores and macropores, Langmuir 15 (1999) 6728–6737, http://dx.doi.org/10.1021/LA990510T.

[85] S. Monticone, R. Tufeu, A.V. Kanaev, Complex nature of the UV and visible fluorescence of colloidal ZnO nanoparticles, J. Phys. Chem. B 102 (1998) 2854–2862, http://dx.doi.org/10.1021/JP973425P.

[86] A.S. Kumar, N.M. Huang, H.S. Nagaraja, Influence of Sn doping on photoluminescence and photoelectrochemical properties of ZnO nanorod arrays, Electron. Mater. Lett. 10 (2014) 753–758, http://dx.doi.org/10.1007/s13391-014-3348-7.

[87] D.L. Wood, J. Tauc, Weak absorption tails in amorphous semiconductors, Phys. Rev. B 5 (1972) 3144–3151, http://dx.doi.org/10.1103/PhysRevB.5.3144.

[88] C.-K. Lin, D. Zhao, W.-Y. Gao, Z. Yang, J. Ye, T. Xu, Q. Ge, S. Ma, D.-J. Liu, Tunability of band gaps in Metal–organic frameworks, Inorg. Chem. 51 (2012) 9039–9044, http://dx.doi.org/10.1021/ic301189m.

[89] Y. Jiang, J. Huang, M. Hunger, M. Maciejewski, A. Baiker, Comparative studies on the catalytic activity and structure of a Cu-MOF and its precursor for alcoholysis of cyclohexene oxide, Catal. Sci. Technol. 5 (2015) 897–902, http://dx.doi.org/10.1039/C4CY00916A.

[90] H. Ying, M. Xiaoyun, L. Ming, Oxidation of alcohols with hydrogen peroxide in the presence of a new triple-site phosphotungstate, Arkivoc 2012 (2012) 187–197, http://dx.doi.org/10.3998/ark.5550190.0013.817.

[91] R. Abdullah Mirzaie, F. Kamrani, A. Anaraki Firooz, A.A. Khodadadi, Effect of α-Fe2O3 addition on the morphological, optical and decolorization properties of ZnO nanostructures, Mater. Chem. Phys. 133 (2012) 311–316, http://dx.doi.org/10.1016/j.matchemphys.2012.01.029.

[92] J. Wang, R. Li, Z. Zhang, W. Sun, R. Xu, Y. Xie, Z. Xing, X. Zhang, Efficient photocatalytic degradation of organic dyes over titanium dioxide coating

upconversion luminescence agent under visible and sunlight irradiation, Appl. Catal. A Gen. 334 (2008) 227–233, http://dx.doi.org/10.1016/j.apcata.2007.10.009.

[93] C. Jiang, B. Fu, H. Cai, T. Cai, Efficient adsorptive removal of Congo red from aqueous solution by synthesized zeolitic imidazolate framework-8, Chem. Speciat. Bioavailab. 28 (2016) 199–208, http://dx.doi.org/10.1080/09542299.2016.1224983.

[94] N. Muhd Julkapli, S. Bagheri, S. Bee Abd Hamid, Recent advances in heterogeneous photocatalytic decolorization of synthetic dyes, Sci. World J. 2014 (2014) 692307, http://dx.doi.org/10.1155/2014/692307.

[95] J. Sun, Y. Wang, R. Sun, S. Dong, Photodegradation of azo dye Congo Red from aqueous solution by the WO3–TiO2/activated carbon (AC) photocatalyst under the UV irradiation, Mater. Chem. Phys. 115 (2009) 303–308, http://dx.doi.org/10.1016/j.matchemphys.2008.12.008.

[96] E.M. Saggioro, A.S. Oliveira, T. Pavesi, C.G. Maia, L.F.V. Ferreira, J.C. Moreira, Use of titanium dioxide photocatalysis on the remediation of model textile wastewaters containing azo dyes, Molecules 16 (2011) 10370–10386, http://dx.doi.org/10.3390/molecules161210370.